

Growth and characterization of Bi(110)/$CrTe_2$ heterostructures: Exploring interplay between magnetism and topology

Zhenyu Yuan(袁震宇), Fazhi Yang(杨发枝), Baiqing Lv(吕佰晴), Yaobo Huang(黄耀波), Tian Qian(钱天), Jinpeng Xu(徐金朋), and Hong Ding(丁洪)

Citation: Chin. Phys. B, 2024, 33 (**2**): 026802. DOI: 10.1088/1674-1056/ad082a
Journal homepage: http://cpb.iphy.ac.cn; http://iopscience.iop.org/cpb

What follows is a list of articles you may be interested in

Adsorption structure of macrocyclic energetic molecule DOATF on Au(111)

Xiao Chang(常霄), Li Huang(黄立), Yixuan Gao(高艺璇), Changjiang Yu(于长江), Yun Cao(曹云), Long Lv(吕龙), Xiao Lin(林晓), Shixuan Du(杜世萱), and Hong-Jun Gao(高鸿钧)
Chin. Phys. B, 2023, 32 (**9**): 096802. DOI: 10.1088/1674-1056/acda84

Phase transition-induced superstructures of *β*-Sn films with atomic-scale thickness

Le Lei(雷乐), Feiyue Cao(曹飞跃), Shuya Xing(邢淑雅), Haoyu Dong(董皓宇), Jianfeng Guo(郭剑锋), Shangzhi Gu(顾尚志), Yanyan Geng(耿燕燕), Shuo Mi(米烁), Hanxiang Wu(吴翰翔), Fei Pang(庞斐), Rui Xu(许瑞), Wei Ji(季威), and Zhihai Cheng(程志海)
Chin. Phys. B, 2021, 30 (**9**): 096804. DOI: 10.1088/1674-1056/ac11e8

Epitaxial growth of antimony nanofilms on HOPG and thermal desorption to control the film thickness

Shuya Xing(邢淑雅), Le Lei(雷乐), Haoyu Dong(董皓宇), Jianfeng Guo(郭剑峰), Feiyue Cao(曹飞跃), Shangzhi Gu(顾尚志), Sabir Hussain, Fei Pang(庞斐), Wei Ji(季威), Rui Xu(许瑞), Zhihai Cheng(程志海)
Chin. Phys. B, 2020, 29 (**9**): 096801. DOI: 10.1088/1674-1056/aba27c

Triphenylene adsorption on Cu(111) and relevant graphene self-assembly

Qiao-Yue Chen(陈乔悦), Jun-Jie Song(宋俊杰), Liwei Jing(井立威), Kaikai Huang(黄凯凯), Pimo He(何丕模), Hanjie Zhang(张寒洁)
Chin. Phys. B, 2020, 29 (**2**): 026801. DOI: 10.1088/1674-1056/ab6583

Adsorption behavior of triphenylene on Ru(0001) investigated by scanning tunneling microscopy

Li-Wei Jing(井立威), Jun-Jie Song(宋俊杰), Yu-Xi Zhang(张羽溪), Qiao-Yue Chen(陈乔悦), Kai-Kai Huang(黄凯凯), Han-Jie Zhang(张寒洁), Pi-Mo He(何丕模)
Chin. Phys. B, 2019, 28 (**7**): 076801. DOI: 10.1088/1674-1056/28/7/076801

Growth and characterization of Bi(110)/$CrTe_2$ heterostructures: Exploring interplay between magnetism and topology

Zhenyu Yuan(袁震宇)[1,2], Fazhi Yang(杨发枝)[1,2], Baiqing Lv(吕佰晴)[3], Yaobo Huang(黄耀波)[4], Tian Qian(钱天)[1,5], Jinpeng Xu(徐金朋)[1,2,6,7,†], and Hong Ding(丁洪)[3,6]

[1] *Beijing National Laboratory for Condensed Matter Physics, Institute of Physics, Chinese Academy of Sciences (CAS), Beijing* 100190, *China*
[2] *School of Physical Sciences, University of Chinese Academy of Sciences, Beijing* 100190, *China*
[3] *Tsung-Dao Lee Institute and School of Physics and Astronomy, Shanghai Jiao Tong University, Shanghai* 200240, *China*
[4] *Shanghai Synchrotron Radiation Facility, Shanghai Advanced Research Institute, Chinese Academy of Sciences, Shanghai* 201204, *China*
[5] *Songshan Lake Materials Laboratory, Dongguan* 523808, *China*
[6] *CAS Center for Excellence in Topological Quantum Computation, University of Chinese Academy of Sciences, Beijing* 100190, *China*
[7] *School of Physics, Shandong University, Ji'nan* 250100 *China*

(Received 14 September 2023; revised manuscript received 20 October 2023; accepted manuscript online 31 October 2023)

The interplay between topology and magnetism is vital for realizing exotic quantum phenomena, significant examples including quantum anomalous Hall effect, axion insulators, and high-order topological states. These states host great potential for future applications in high-speed and low-consumption electronic devices. Despite being extensively investigated, practical platforms are still scarce. In this work, with molecular beam epitaxy (MBE), we provide the first experimental report on high-quality Bi(110)/$CrTe_2$ magnetic heterostructure. By employing *in-situ* high-resolution scanning tunneling microscopy, we are able to examine the interaction between magnetism and topology. There is a potential edge state at an energy level above the Fermi level, but no edge states observed near the Fermi level The absence of high-order topological corner states near E_F highlights the importance of lattice matching and interface engineering in designing high-order topological states. Our study provides key insights into the interplay between two-dimensional magnetic and topological materials and offers an important dimension for engineering magnetic topological states.

Keywords: bismuth (110), chromium ditelluride ($CrTe_2$), topological states, scanning tunneling microscopy (STM)

PACS: 68.60.–p, 73.90.+f, 73.22.–f, 75.75.Lf **DOI:** 10.1088/1674-1056/ad082a

1. Introduction

Condensed matter physics has witnessed remarkable advancements driven by evolutionary concepts.[1] The discovery of the KT phase transition[2] and the integer and fractional quantum Hall effect[3,4] ignited a surge of interest in studying topological states of matter in condensed matter physics. To date, numerous topologically non-trivial materials have been predicted,[5–7] solidifying the research of topological states of matter as a notable frontier and hotspot within the field. The distinctive "bulk–boundary correspondence" in topological quantum matter offers immense potential for various applications, such as nondissipative transport enabled by topological protection.

Bismuth has long been a focal point of research due to its robust spin–orbit coupling and layer-dependent energy bands. Recent experiments and theories have suggested that bulk bismuth may possess characteristics of a high-order topological insulator,[8–10] albeit with some potential disputes.[11] Furthermore, two-dimensional (2D) topological insulators are more practical than their three-dimensional (3D) counterparts due to their one-dimensional (1D) nondissipative conductive channels. Currently, several 2D topological insulators have been discovered, such as HgTe/CdTe quantum wells,[12] InAs/GaSb/InAs triple quantum wells,[13] Bismuthene on an SiC substrate,[14] monolayer 1T′-WTe_2,[15,16] and so on. However, comprehensive experimental evidence[17–23] supports that a 2D bismuth film can exhibit properties of a 2D topological insulator. Thus, further detailed experimental explorations are highly anticipated to shed light on this exciting area of research. Undoubtedly, bismuth is a material that exhibits a rich variety of topological states, and its combination with magnetism presents an exceptionally enticing direction. Additionally, in recent years, heterojunctions formed by coupling topological insulators with other materials have revealed a host of surprising physical phenomena. For example, the heterojunction formed by combining Bi_2Te_3 and $NbSe_2$ exhibits properties of topological superconductivity,[24–26] while the coupling of FeTe and Bi_2Te_3 in a heterojunction demonstrates interfacial superconductivity.[26–28] Therefore, exploring the physical properties of heterojunctions between topological insulators and other materials holds immense value in unraveling potential physical phenomena. In summary, exploring the convergence of topologically diverse materials, like bismuth, with magnetism, and investigating heterojunc-

[†]Corresponding author. E-mail: xujp@iphy.ac.cn

© 2024 Chinese Physical Society and IOP Publishing Ltd

tions between topological insulators and other substances, offer intriguing avenues of research with significant potential for discoveries.

In recent years, there has been a multitude of 2D magnetic materials that have been discovered which are particularly attractive due to their potential application value in atomic-level spintronic devices.[29–35] $CrTe_2$ is a rare magnetic material that surprisingly maintains its ferromagnetism at room temperature.[36–39] Additionally, in-plane antiferromagnetism appears when it has only one atomic layer $CrTe_2$,[40] possibly related to the stress generated between epitaxial growth and the substrate.[41] The abundant and valuable physical properties exhibited by 2D magnetic materials, coupled with their ability to form heterostructures with other materials, render them an excellent platform for investigating the interplay between magnetism and other materials.[42,43] For example, the ferromagnetism of $CrTe_2$, the strong spin–orbit coupling of Bi_2Te_3, and the atomically flat interface of the two two-dimensional materials, make it possible to obtain a strong Dzyaloshinskii–Moriya interaction (DMI) in the $CrTe_2/Bi_2Te_3$ heterostructure. This interaction results in spatial spin modulations and topological Hall effects, indicating the emergence of interfacial Skyrmions.[44,45] It is also predicted that combining the Curie temperature at room temperature of $CrTe_2$ with the rich topological properties of Bi could lead to interesting physical phenomena, such as the quantum anomalous Hall effect.[46–48]

In the present study, we employed molecular beam epitaxy (MBE) to grow multilayer $CrTe_2$, which was confirmed through RHEED and scanning tunneling microscopy. Based on this, we achieved the first-ever growth of a $Bi/CrTe_2$ heterojunction. By utilizing scanning tunneling microscopy, we determined the orientation of the Bi islands to be along the (110) direction. Then we performed a comprehensive characterization of the heterostructure using scanning tunneling microscopy to probe its topological properties in the context of potential 2D topological and 2D magnetic interactions. Our detailed investigations suggest no substantial evidence of noteworthy edge states near the Fermi level within the Bi islands. This can be attributed to the complicated interplay between the $CrTe_2$ magnetic substrate and the Bi islands themselves, including potential influences from strain and magnetic exchange interactions. Nonetheless, there are potential edge states positioned above the Fermi level, a phenomenon reminiscent of the observations in a prior study.[21] Furthermore, we proposed that the growth of heterostructure thin films of Bi on magnetic substrates with smaller lattice constants can effectively induce the coupling between magnetic and topological states in Bi.

2. Methods

The experiment was performed using the MBE–STM joint system of Unisoku 1300. MBE was equipped with RHEED to enable real-time monitoring of the sample growth process. The growth of $CrTe_2$ on treated bilayer graphene substrates was carried out using MBE. The substrate was a single-sided polished 4H–SiC (0001) produced by TankeBlue Semiconductor. To form the bilayer graphene, the substrate was degassed at 600 °C for 6 hours, and then flashed 30 times at 1150 °C for 15 seconds to remove silicon atoms from the SiC surface. The flux ratio to grow $CrTe_2$, with Cr to Te in a ratio of 1:30, was maintained while the substrate was kept at 365 °C. The grown $CrTe_2$ multilayers were cooled to approximately 130 K using liquid nitrogen to enable Bi deposition and the formation of Bi islands. After further annealing, small Bi islands were aggregated into larger ones. The vacuum degree of all MBE growth processes was maintained at 1×10^{-9} Torr ($1\ \text{Torr} = 1.33322 \times 10^2$ Pa) or better. The ultra-high resolution STM/STS measurements were performed at a liquid helium temperature of 4.2 K or 77 K under vacuum conditions better than 1×10^{-9} Torr. Tungsten or PtIr tips were used for measurements, and the measured bias was the voltage of the sample relative to the grounded tip. The STM images were processed using Gwyddion software.

3. Results and discussion

Figure 1(a) displays the RHEED diffraction pattern of bilayer graphene after annealing 4H–SiC. The pattern exhibits high clarity, indicating the purity and flatness of the substrate. Figure 1(b) shows the RHEED diffraction pattern of $CrTe_2$ grown on bilayer graphene. The diffraction fringes are well-defined, signifying excellent crystallinity and flatness of the film. A weaker fringe at the middle of the first-order diffraction fringe and the zero-order fringe (white arrow) is attributable to the 2×1 reconstruction, which similar with the observation in a pervious report.[40] The double lines near the second-order diffraction fringes (red arrows) suggest two orientations of $CrTe_2$ on bilayer graphene. In Fig. 1(c), the RHEED pattern of Bi deposited on $CrTe_2$ is displayed, where the deposition process leads to the blurring of the original diffraction fringes. Simultaneously, a new diffraction fringe emerges at the location indicated by the white arrow. Combining the relative orientation of Bi and $CrTe_2$ as characterized by STM (Fig. 1(d)), it can be confirmed through calculations that the diffraction fringes at this position originate from the Bi film. Additionally, the incomplete coverage of Bi on the surface and the existence of depressions in $CrTe_2$ facilitate the deposition and crystallization of Bi within these depressions, which can elucidate the blur of its distinctive pattern.

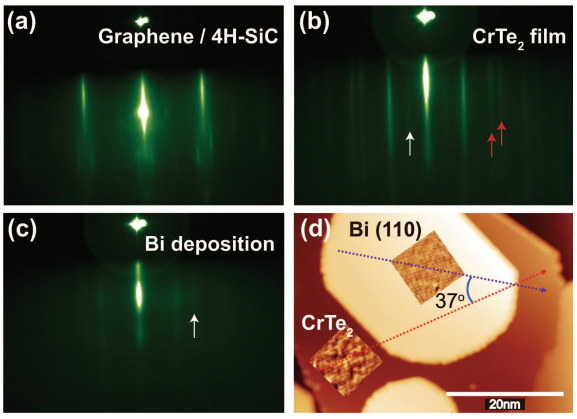


Fig. 1. The RHEED diffraction patterns were obtained for (a) flat bilayer graphene on 4H-SiC substrate, (b) $CrTe_2$ film grown on bilayer graphene. The red arrows in panel (b) indicate two orientations of $CrTe_2$, and the white arrows indicate 2×1 reconstruction. (c) Bi deposited on $CrTe_2$. The position indicated by the white arrow in panel (c) corresponds to the newly crystallized Bi film. (d) displays the sample morphology characterized by STM, showing an approximate 37° angle between the Bi island lattice orientation and the $CrTe_2$ lattice orientation.

We employed low-temperature high-resolution scanning tunneling microscopy (STM/STS) to confirm the quality of the thin films and study at the atomic scale. Figure 2(a) displays a large-scale (300 nm × 300 nm) topography of bilayer graphene annealed on 4H-SiC. The sample surface exhibits a clear atomicresolved hexagonal lattice structure, depicted in Fig. 2(b). Additionally, the Moiré pattern produced by the stacked graphene is evident due to the flatness of the surface. Figure 2(c) exhibits the large-scale topography of $CrTe_2$, indicating a flat surface with no higher layers except the second layer, indicating a layer-by-layer growth mode. The step height is approximately 62 Å, which is consistent with previous reports.[44] The corresponding atomic resolution image, shown in Fig. 2(d), also displays a well-resolved hexagonal lattice, with a lattice constant of 3.87 Å, consistent with previous reports.[40,44] Figure 2(e) is a large-scale topography of Bi islands deposited on $CrTe_2$, indicating a clean surface with large and smooth deposited Bi islands, showing a high heterostructure quality. The atomic resolution of the corresponding Bi islands, shown in Fig. 2(f), shows a clear near-tetragonal structure, which is the Bi(110) plane as shown in previous studies.[23,49–54] The measured lattice constants are 4.71 Å and 4.35 Å, similar to the previous report,[50] with the step height being around 750 Å, which is comparable to the previous report.[51,54] A lattice diagram of Bi(110) deposited on $CrTe_2$, created using VESTA software,[55] is shown in Fig. 2(g). The electronic local density of state on $CrTe_2$ and Bi(110) in the heterostructure structure is depicted in Figs. 2(h) and 2(i), respectively. It shows that $CrTe_2$ displays good metallic density of states, in line with previous reports,[40,44] which indicates a similar magnetic structure in our $CrTe_2$ films The Bi(110) films exhibit good metal conduction under the effect of heterointerface, which indicates that the neighbor interaction between heterostructures is strong enough to have a significant impact.

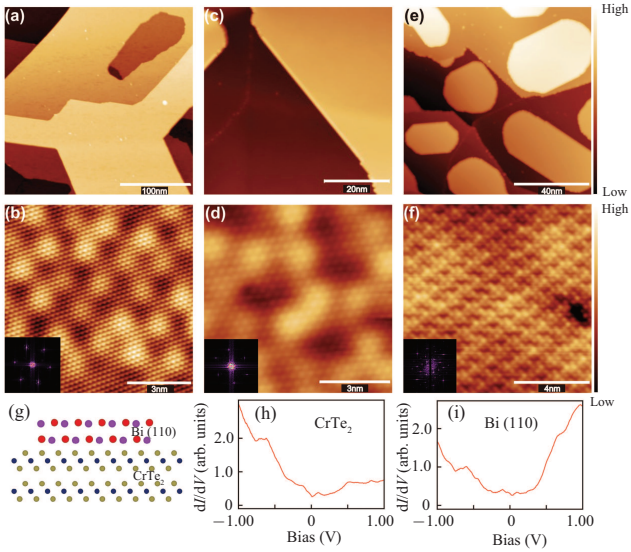


Fig. 2. Atomic-scale imaging and spectroscopic characterization of the thin films. (a) Large-scale topography of bilayer graphene annealed on 4H-SiC ($V_b = 1$ V, $I_{set} = 50$ pA). (b) Atomic-resolution image of bilayer graphene showing hexagonal symmetry (inset) and Moiré period modulation ($V_b = 100$ mV, $I_{set} = 400$ pA). (c) Large-scale topography of $CrTe_2$ indicating a layer-by-layer growth mode ($V_b = 1$ V, $I_{set} = 50$ pA). (d) Atomic-resolution image of $CrTe_2$ showing hexagonal symmetry (inset) and a lattice constant of 3.87 Å. ($V_b = -500$ mV, $I_{set} = 500$ pA). (e) Large-scale topography of Bi islands deposited on $CrTe_2$ indicating a high-quality heterojunction ($V_b = 1$ V, $I_{set} = 400$ pA). (f) Atomic-resolution image of Bi islands showing a clear near-tetragonal structure corresponding to the Bi(110) plane with a lattice constant of 4.71 Å and 4.35 Å. ($V_b = -50$ mV, $I_{set} = 600$ pA). (g) Model diagram of Bi(110) deposited on $CrTe_2$. (h) and (i) Electronic localized density of state spectra on $CrTe_2$ and Bi(110) in the heterojunction structure, respectively, indicating strong neighbor interaction between heterojunctions.

After verifying the quality of the heterostructures, we focus on exploring the interplay between the 2D magnetism of $CrTe_2$ and the topological properties of Bi(110). As shown in Fig. 3, we investigated two Bi(110) islands with sizes larger than 20 nm to examine the changes in their supposed edge states with the participation of magnetic neighbors. Figure 3(a) displays the topography of a Bi(110) island on $CrTe_2$, which forms a lateral heterostructure with $CrTe_2$ along the in-plane direction due to the barrier of the boundary of the second layer of $CrTe_2$.

In Fig. 3(b), we collected the density of states of multiple points along the direction of the blue arrow in Fig. 3(a) aligning with the $[01\bar{1}]$ direction of Bi(110). It can be observed that the density of state significantly changes at the step of Bi(110), as indicated by the yellow dotted line in the figure. The density of state at negative voltage bias exhibits an overall significant decrease at one edge (blue), while the other edge (red) does not experience such a reduction, which could be attributed to the atomic buckling effect.[54] However, unlike the previously observed edge states on Bi(110) or Bi(111),[9,10,18,21,56] we did not find any significant edge states on the step near the Fermi level in our measurements. Meanwhile, we observed an enhancement of the density of state around 350 meV at the step

edge, which is distinct from the bulk state. This phenomenon is also clearly demonstrated in Figs. 4(c)–4(e). We obtained results shown in Figs. 3(c) and 3(d) at another Bi(110) island with the same method, which are consistent with Figs. 3(a) and 3(b), demonstrating the robustness of our findings. We will comprehensively discuss these phenomena later.

Additionally, we observed intriguing yet unexplained phenomena in the measurements depicted in Fig. 3. It is noteworthy that a significant enhancement in the density of states appears on the bulk states of Bi(110) at an energy of about 100 meV. This energy position aligns precisely with the energy at which the topological edge state of Bi(110) was reported in previous studies.[10,23] However, this enhancement of the density of state is not observed at the step edge. Furthermore, on the underlying $CrTe_2$, there is also an increase in the density of state at the close energy level. Although we believe that the underlying mechanism of this phenomenon is closely related to the 2D magnetic properties of $CrTe_2$ and the topological properties of Bi(110), further investigations are necessary to clarify it.

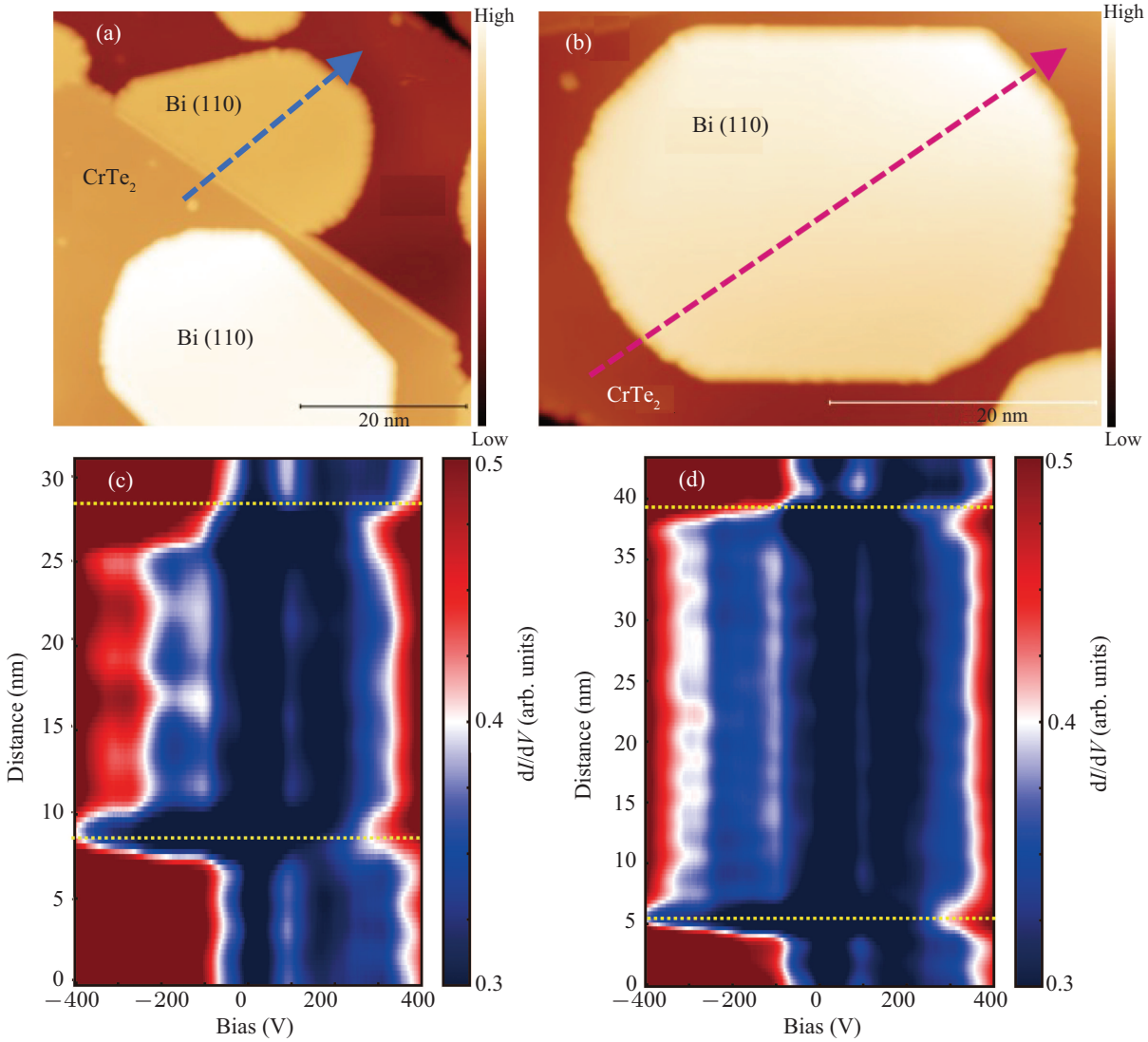


Fig. 3. Exploration of the changes in the boundary state of Bi(110) on $CrTe_2$. (a) Morphology of a Bi(110) island on $CrTe_2$, forming a transverse heterojunction in the in-plane direction. ($V_b = 1$ V, $I_{set} = 50$ pA). (b) Density of states of multiple points along the direction of the arrow in panel (a), showing significant changes in the density of states spectrum at the step of Bi(110) (marked by the yellow dotted line), but no significant edge states were found. (c) and (d) Results consistent with panels (a) and (b), confirming the robustness of the findings.

In our few layers $CrTe_2$ case, there should be some in-plane magnetism component because the in-plane nature of magnetism in monolayer $CrTe_2$. There are some theoretical proposals[57] that if the edge state near the Fermi level of the topologically non-trivial Bi(110) is gapped due to the potential existence of an in-plane ferromagnetic component in $CrTe_2$, it would give rise to corner states associated with high-order topological states. To investigate this possibility, we performed an detailed mapping near the boundary, as depicted in Fig. 4.

Figure 4(a) displays the location and size of the Bi(110) islands selected for mapping, while figure 4(b) shows the topography of the blue box part in Fig. 4(a). The sharp edges of the island prevent complex scattering effects caused by

rough edges and impurities. Additionally, the use of 50 nm-scale islands avoids the change in the density of states caused by finite size effects from the small area of the island. Figures 4(c)–4(h) display density of state mappings at several selected energy levels, with the corresponding color bar positioned on the right side of the figure. At higher energy levels (Figs. 4(c)–4(e)), an about 2 nm-wide edge state is evident at the step edge, a phenomenon strikingly akin to the topological edge states above the Fermi level previously reported in Bi(111).[21] Hence, there is a strong possibility that this may indeed represent a nontrivial topological edge state above the Fermi level. Furthermore, our density of states mapping results did not reveal any evidence of topological corner states in Bi(110)/$CrTe_2$ films, as shown in Figs. 4(c)–4(h). This indicates that the weak coupling between in-plane magnetic and topological edge states in this magnetic heterostructure.

Although theoretical predictions have suggested the possible topological edge states near the Fermi level in the Bi(110) system, our experimental findings indicate the absence of such topological edge states near the Fermi level in the Bi(110)/$CrTe_2$ magnetic heterostructure. Instead our observations suggest the potential presence of edge states similar with the topological edge states found in the Bi(111) system at a higer energy positions. In the theoretical predictions, the black phosphorus (BP) phase structure of Bi(110) was deemed crucial for the formation of topological states. This suggests that the significant lattice mismatch in the Bi(110)/$CrTe_2$ heterostructure may have an impact on the BP structure of Bi(110), which disrupts the expected topological edge states near the Fermi level. Therefore, the lattice constant of magnetic substrate is important for the high-quality Bi(110) films with the BP structure. In order to minimize the influence of buckling, substrates with a high density of state near the Fermi level should be chosen. Table 1 presents a list of experimentally verified 2D magnetic materials that could serve as potential options for magnetic substrates in constructing high-order topological magnetic heterostructures with 2D Bi.

Table 1. Experimentally confirmed typical 2D ferromagnetic materials and their lattice constants.

Category	Materials	Magnetism	Gap (eV)	Lattice constant (Å)
Transition metal halides	$CrBr_3$	⊥ FM	2.2	6.38[58]
	$CrTe_2$	⊥ FM	0	3.77[59]
Transition metal sulfides	1T-VSe_2	⊥ FM	0	3.33[60]
	Cr_2S_3	FM	0	6.03[61]
Transition metal germanides	$Cr_2Si_2Te_6$	⊥ FM	1.2	6.76[62]
	$Cr_2Ge_2Te_6$	⊥ FM	0.45	6.83[62]
	Fe_3GeTe_2	⊥ FM	0	3.95[63]
	Fe_5GeTe_2	⊥ FM	0	4.05[64]

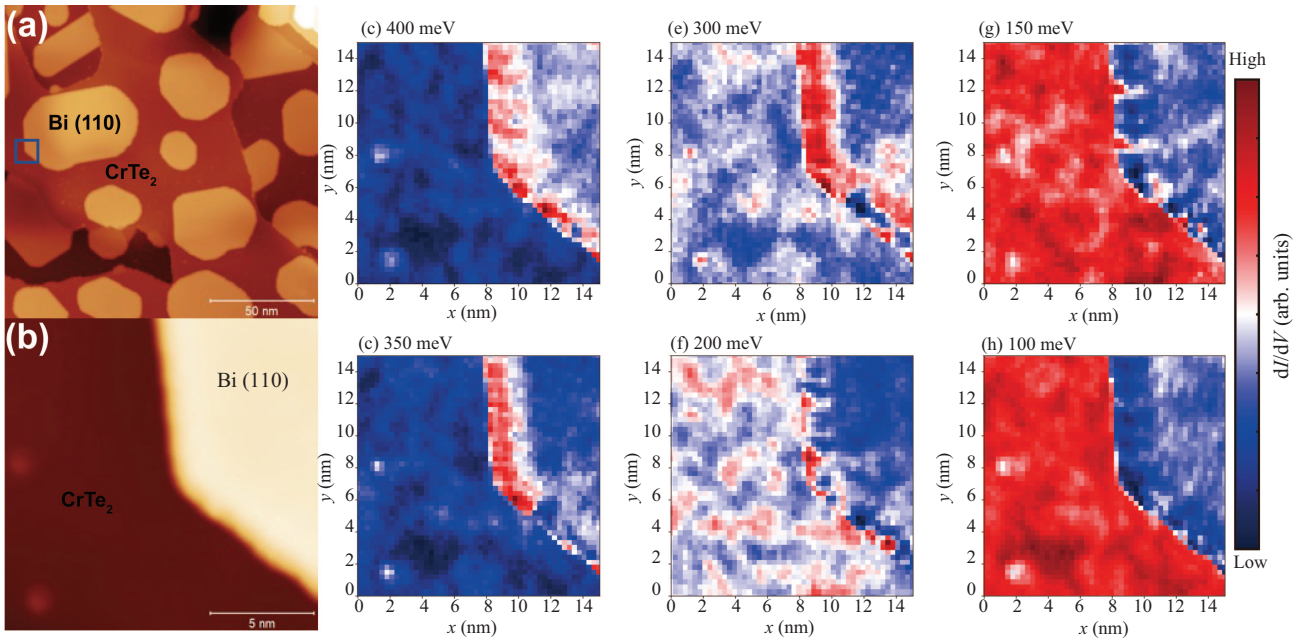


Fig. 4. Detailed mapping near the boundary of Bi(110) islands. (a) Location and size of the selected islands for mapping (V_b = 1 V, I_{set} = 50 pA). (b) Morphology of the blue box part in panel (a), showing the sharp edges of the island (V_b = 500 mV, I_{set} = 500 pA). (c)–(h) Density of state mapping at selected energies, indicating the energy range in which the density of state is transferred. The color bar is consistent with that used in Fig. 3.

4. Conclusions

In conclusion, we have grown a high-quality Bi(110)/$CrTe_2$ magnetic heterostructure and investigated its electronic properties along with potential topological characteristics. Our findings suggest the absence of topological edge states near the Fermi level, possibly due to the significant lattice mismatch. However, we have discovered an engaging edge state at higher energy positions on the Bi(110) surface which bears a resemblance to the topological edge state previously reported on the Bi(111) surface.[21] This could be a consequence of interplay between magnetism and topology, necessitating further theoretical investigation of this magnetic heterostructure system. To mitigate lattice mismatch and better realize the interplay between magnetism and bismuth's topological states, we propose several alternative magnetic substrate materials that are more suitable for growing magnetic heterostructures. This study provides a foundation for future research in the fields of topological insulators, two-dimensional magnetism, and heterostructure physics.

Acknowledgments

We would like to express our gratitude to Guang Bian from the University of Missouri, and to Xiaoqian Zhang from Southern University of Science and Technology for their valuable discussions and insights.

The work at IOP is supported by grants from the National Natural Science Foundation of China (Grant No. U2032204), the Ministry of Science and Technology of China (Grant No. 2022YFA1403800), and the Chinese Academy of Sciences (Grant No. XDB33000000).

References

[1] Anderson P W 1972 *Science* **177** 393
[2] Kosterlitz J M and Thouless D J 1973 *J. Phys. C: Solid State Phys.* **6** 1181
[3] Klitzing K V, Dorda G and Pepper M 1980 *Phys. Rev. Lett.* **45** 494
[4] Tsui D C, Stormer H L and Gossard A C 1982 *Phys. Rev. Lett.* **48** 1559
[5] Zhang T, Jiang Y, Song Z, Huang H, He Y, Fang Z, Weng H and Fang C 2019 *Nature* **566** 475
[6] Vergniory M G, Elcoro L, Felser C, Regnault N, Bernevig B A and Wang Z 2019 *Nature* **566** 480
[7] Tang F, Po H C, Vishwanath A and Wan X 2019 *Nature* **566** 486
[8] Schindler F, Wang Z J, Vergniory M G, Cook A M, Murani A, Sengupta S, Kasumov A Y, Deblock R, Jeon S, Drozdov I, Bouchiat H, Guéron S, Yazdani A, Bernevig B A and Neupert T 2018 *Nat. Phys.* **14** 918
[9] Drozdov I K, Alexandradinata A, Jeon S, Nadj-Perge S, Ji H, Cava R J, Andrei Bernevig B and Yazdani A 2014 *Nat. Phys.* **10** 664
[10] Aggarwal L, Zhu P, Hughes T L and Madhavan V 2021 *Nat. Commun.* **12** 4420
[11] Nayak A K, Reiner J, Queiroz R, Fu H, Shekhar C, Yan B, Felser C, Avraham N and Beidenkopf H 2019 *Sci. Adv.* **5** eaax6996
[12] König M, Wiedmann S, Brüne C, Roth A, Buhmann H, Molenkamp L W, Qi X L and Zhang S C 2007 *Science* **318** 766
[13] Meyer M, Schmid S, Jabeen F, Bastard G, Hartmann F and Höfling S 2021 *Phys. Rev. B* **104** 085301
[14] Reis F, Li G, Dudy L, Bauernfeind M, Glass S, Hanke W, Thomale R, Schäfer J and Claessen R 2017 *Science* **357** 287
[15] Tang S, Zhang C, Wong D, Pedramrazi Z, Tsai H Z, Jia C, Moritz B, Claassen M, Ryu H, Kahn S, Jiang J, Yan H, Hashimoto M, Lu D, Moore R G, Hwang C C, Hwang C, Hussain Z, Chen Y, Ugeda M M, Liu Z, Xie X, Devereaux T P, Crommie M F, Mo S K and Shen Z X 2017 *Nat. Phys.* **13** 683
[16] Wu S, Fatemi V, Gibson Q D, Watanabe K, Taniguchi T, Cava R J and Jarillo-Herrero P 2018 *Science* **359** 76
[17] Kundu A K, Gu G and Valla T 2021 *ACS Appl. Mater. Interfaces* **13** 33627
[18] Gao C L, Qian D, Liu C H, Jia J F and Liu F 2013 *Chin. Phys. B* **22** 067304
[19] Peng L, Xian J J, Tang P, Rubio A, Zhang S C, Zhang W and Fu Y S 2018 *Phys. Rev. B* **98** 245108
[20] Wells J W, Dil J H, Meier F, Lobo-Checa J, Petrov V N, Osterwalder J, Ugeda M M, Fernandez-Torrente I, Pascual J I, Rienks E D L, Jensen M F and Hofmann Ph 2009 *Phys. Rev. Lett.* **102** 096802
[21] Yang F, Miao L, Wang Z F, Yao M Y, Zhu F, Song Y R, Wang M X, Xu J P, Fedorov A V, Sun Z, Zhang G B, Liu C, Liu F, Qian D, Gao C L and Jia J F 2012 *Phys. Rev. Lett.* **109** 016801
[22] Yao M Y, Zhu F, Han C Q, Guan D D, Liu C, Qian D and Jia J 2016 *Sci. Rep.* **6** 21326
[23] Lu Y, Xu W, Zeng M, Yao G, Shen L, Yang M, Luo Z, Pan F, Wu K, Das T, He P, Jiang J, Martin J, Feng Y P, Lin H and Wang X 2015 *Nano Lett.* **15** 80
[24] Xu J P, Liu C, Wang M X, Ge J, Liu Z L, Yang X, Chen Y, Liu Y, Xu Z A, Gao C L, Qian D, Zhang F C and Jia J F 2014 *Phys. Rev. Lett.* **112** 217001
[25] Xu J P, Wang M X, Liu Z L, Ge J F, Yang X, Liu C, Xu Z A, Guan D, Gao C L, Qian D, Liu Y, Wang Q H, Zhang F C, Xue Q K and Jia J F 2015 *Phys. Rev. Lett.* **114** 017001
[26] Wang M X, Liu C, Xu J P, Yang F, Miao L, Yao M Y, Gao C L, Shen C, Ma X, Chen X, Xu Z A, Liu Y, Zhang S C, Qian D, Jia J F and Xue Q K 2012 *Science* **336** 52
[27] Qin H, Chen X, Guo B, Pan T, Zhang M, Xu B, Chen J, He H, Mei J, Chen W, Ye F and Wang G 2021 *Nano Lett.* **21** 1327
[28] He Q L, Liu H, He M, Lai Y H, He H, Wang G, Law K T, Lortz R, Wang J and Sou I K 2014 *Nat. Commun.* **5** 4247
[29] Novoselov K S, Geim A K, Morozov S V, Jiang D, Zhang Y, Dubonos S V, Grigorieva I V and Firsov A A 2004 *Science* **306** 666
[30] Sangwan V K and Hersam M C 2018 *Ann. Rev. Phys. Chem.* **69** 299
[31] Wang Q H, Kalantar-Zadeh K, Kis A, Coleman J N and Strano M S 2012 *Nat. Nanotech.* **7** 699
[32] Wang W, Wu X and Zhang J 2015 *J. Nanomater.* **2015** e198126
[33] Zhang X, Hou L, Ciesielski A and Samorì P 2016 *Adv. Energy Mater.* **6** 1600671
[34] Jiang X H, Qin S C, Xing Z Y, Zou X Y, Deng Y F, Wang W and Wang L 2021 *Acta Phys. Sin.* **70** 127801 (in Chinese)
[35] Xiao H, Mi M J and Wang Y L 2021 *Acta Phys. Sin.* **70** 127503 (in Chinese)
[36] Freitas D C, Weht R, Sulpice A, Remenyi G, Strobel P, Gay F, Marcus J and Núñez-Regueiro M 2015 *J. Phys.: Condens. Matter* **27** 176002
[37] Zhang X, Lu Q, Liu W, Niu W, Sun J, Cook J, Vaninger M, Miceli P F, Singh D J, Lian S W, Chang T R, He X, Du J, He L, Zhang R, Bian G and Xu Y 2021 *Nat. Commun.* **12** 2492
[38] Chua R, Zhou J, Yu X, Yu W, Gou J, Zhu R, Zhang L, Liu M, Breese M B H, Chen W, Loh K P, Feng Y P, Yang M, Huang Y L and Wee A T S 2021 *Adv. Mater.* **33** 2103360
[39] Sun X, Li W, Wang X, Sui Q, Zhang T, Wang Z, Liu L, Li D, Feng S, Zhong S, Wang H, Bouchiat V, Nunez Regueiro M, Rougemaille N, Coraux J, Purbawati A, Hadj-Azzem A, Wang Z, Dong B, Wu X, Yang T, Yu G, Wang B, Han Z, Han X and Zhang Z 2020 *Nano Res.* **13** 3358
[40] Xian J J, Wang C, Nie J H, Li R, Han M, Lin J, Zhang W H, Liu Z Y, Zhang Z M, Miao M P, Yi Y, Wu S, Chen X, Han J, Xia Z, Ji W and Fu Y S 2022 *Nat. Commun.* **13** 257
[41] Lv H Y, Lu W J, Shao D F, Liu Y and Sun Y P 2015 *Phys. Rev. B* **92** 214419
[42] Butler S Z, Hollen S M, Cao L, Cui Y, Gupta J A, Gutiérrez H R, Heinz T F, Hong S S, Huang J, Ismach A F, Johnston-Halperin E, Kuno M, Plashnitsa V V, Robinson R D, Ruoff R S, Salahuddin S, Shan J, Shi L, Spencer M G, Terrones M, Windl W and Goldberger J E 2013 *ACS Nano* **7** 2898
[43] Gibertini M, Koperski M, Morpurgo A F and Novoselov K S 2019 *Nat. Nanotechnol.* **14** 408

[44] Zhang X, Ambhire S C, Lu Q, Niu W, Cook J, Jiang J S, Hong D, Alahmed L, He L, Zhang R, Xu Y, Zhang S L, Li P and Bian G 2021 *ACS Nano* **15** 15710

[45] Nie J, Li R, Miao M, Fu Y and Zhang W 2023 *Materials Futures* **2** 021001

[46] Qi X L, Wu Y S and Zhang S C 2006 *Phys. Rev. B* **74** 085308

[47] Qi X L, Hughes T L and Zhang S C 2008 *Phys. Rev. B* **78** 195424

[48] Nomura K and Nagaosa N 2011 *Phys. Rev. Lett.* **106** 166802

[49] Wang J, Sun X, Du H, Ma C and Wang B 2022 *Phys. Rev. B* **105** 115407

[50] Sun J T, Huang H, Wong S L, Gao H J, Feng Y P and Wee A T S 2012 *Phys. Rev. Lett.* **109** 246804

[51] Zhang K H L, McLeod I M, Lu Y H, Dhanak V R, Matilainen A, Lahti M, Pussi K, Egdell R G, Wang X S, Wee A T S and Chen W 2011 *Phys. Rev. B* **83** 235418

[52] He B, Tian G, Gou J, Liu B, Shen K, Tian Q, Yu Z, Song F, Xie H, Gao Y, Lu Y, Wu K, Chen L and Huang H 2019 *Surface Science* **679** 147

[53] Jin K H, Oh E, Stania R, Liu F and Yeom H W 2021 *Nano Lett.* **21** 9468

[54] Xi Y, Zhao M, Feng H, Sun Y, Man X, Xu X, Hao W, Dou S and Du Y 2021 *J. Phys.: Condens. Matter* **34** 074003

[55] Momma K and Izumi F 2011 *J. Appl. Crystallogr* **44** 1272

[56] Liu J Y, Sun H H, Guan D D, Li Y Y, Wang S Y, Liu C H, Zheng H and Jia J F 2018 *Acta Phys. Sin.* **67** 170701 (in Chinese)

[57] Chen C, Song Z, Zhao J Z, Chen Z, Yu Z M, Sheng X L and Yang S A 2020 *Phys. Rev. Lett.* **125** 056402

[58] McGuire M A 2017 *Crystals* **7** 121

[59] Meng L, Zhou Z, Xu M, Yang S, Si K, Liu L, Wang X, Jiang H, Li B, Qin P, Zhang P, Wang J, Liu Z, Tang P, Ye Y, Zhou W, Bao L, Gao H J and Gong Y 2021 *Nat. Commun.* **12** 809

[60] Yu W, Li J, Herng T S, Wang Z, Zhao X, Chi X, Fu W, Abdelwahab I, Zhou J, Dan J, Chen Z, Chen Z, Li Z, Lu J, Pennycook S J, Feng Y P, Ding J and Loh K P 2019 *Adv. Mater.* **31** 1903779

[61] Cui F, Zhao X, Xu J, Tang B, Shang Q, Shi J, Huan Y, Liao J, Chen Q, Hou Y, Zhang Q, Pennycook S J and Zhang Y 2020 *Adv. Mater.* **32** 1905896

[62] Ito N, Kikkawa T, Barker J, Hirobe D, Shiomi Y and Saitoh E 2019 *Phys. Rev. B* **100** 060402

[63] Fei Z, Huang B, Malinowski P, Wang W, Song T, Sanchez J, Yao W, Xiao D, Zhu X, May A F, Wu W, Cobden D H, Chu J H and Xu X 2018 *Nat. Mater.* **17** 778

[64] May A F, Ovchinnikov D, Zheng Q, Hermann R, Calder S, Huang B, Fei Z, Liu Y, Xu X and McGuire M A 2019 *ACS Nano* **13** 4436